MNRAS **000**, 1–10 (2022) Preprint 12 June 2022 Compiled using MNRAS LATEX style file v3.0

A 5% measurement of the Hubble-Lemaître constant from Type II supernovae

T. de Jaeger[1]★, L. Galbany[2,3] A. G. Riess[4,5], B. E. Stahl[6], B. J. Shappee[1], A. V. Filippenko[6], W. Zheng[6]

[1]*Institute for Astronomy, University of Hawaii, 2680 Woodlawn Drive, Honolulu, HI 96822, USA.*
[2]*Institute of Space Sciences (ICE, CSIC), Campus UAB, Carrer de Can Magrans, s/n, E-08193 Barcelona, Spain.*
[3]*Institut d'Estudis Espacials de Catalunya (IEEC), E-08034 Barcelona, Spain.*
[4]*Space Telescope Science Institute, 3700 San Martin Drive, Baltimore, MD 21218, USA.*
[5]*Department of Physics & Astronomy, Johns Hopkins University, Baltimore, MD 21218, USA.*
[6]*Department of Astronomy, University of California, Berkeley, CA 94720-3411, USA.*

ABSTRACT

The most stringent local measurement of the Hubble-Lemaître constant from Cepheid-calibrated Type Ia supernovae (SNe Ia) differs from the value inferred via the cosmic microwave background radiation (*Planck*+ΛCDM) by $\sim 5\sigma$. This so-called "Hubble tension" has been confirmed by other independent methods, and thus does not appear to be a possible consequence of systematic errors. Here, we continue upon our prior work of using Type II supernovae to provide another, largely-independent method to measure the Hubble-Lemaître constant. From 13 SNe II with geometric, Cepheid, or tip of the red giant branch (TRGB) host-galaxy distance measurements, we derive $H_0 = 75.4^{+3.8}_{-3.7}\,\mathrm{km\,s^{-1}\,Mpc^{-1}}$ (statistical errors only), consistent with the local measurement but in disagreement by $\sim 2.0\sigma$ with the *Planck*+ΛCDM value. Using only Cepheids ($N = 7$), we find $H_0 = 77.6^{+5.2}_{-4.8}\,\mathrm{km\,s^{-1}\,Mpc^{-1}}$, while using only TRGB ($N = 5$), we derive $H_0 = 73.1^{+5.7}_{-5.3}\,\mathrm{km\,s^{-1}\,Mpc^{-1}}$. Via 13 variants of our dataset, we derive a systematic uncertainty estimate of $1.5\,\mathrm{km\,s^{-1}\,Mpc^{-1}}$. The median value derived from these variants differs by just $0.3\,\mathrm{km\,s^{-1}\,Mpc^{-1}}$ from that produced by our fiducial model. Because we only replace SNe Ia with SNe II — and we do not find statistically significant difference between the Cepheid and TRGB H_0 measurements — our work reveals no indication that SNe Ia or Cepheids could be the sources of the "H_0 tension." We caution, however, that our conclusions rest upon a modest calibrator sample; as this sample grows in the future, our results should be verified.

Key words: cosmology: distance scale – galaxies: distances and redshifts – stars: supernovae: general

1 INTRODUCTION

In the century since Georges Lemaître (Lemaître 1927) and Edwin Hubble (Hubble 1929) discovered that the Universe is expanding, astronomers have made significant strides in measuring its current expansion rate (known as the Hubble-Lemaître constant, H_0). Traditionally, two different approaches have been employed that leverage measurements at opposite extremes of the visible Universe.

(i) With the *distance-ladder method*, relative distances to nearby galaxies in the Hubble flow (i.e., whose motions are mainly due to the expansion of the Universe) are anchored to absolute distance measurements. It is currently comprised of three steps/rungs: (i) geometric distances like Milky Way Cepheid parallaxes from *Gaia* EDR3 (Lindegren et al. 2021; Riess et al. 2021b), detached eclipsing binary stars in the Large Magellanic Cloud (Pietrzyński et al. 2019), or the Keplerian motion of masers in NGC 4258 (Reid et al. 2019; Humphreys et al. 2013) are used to standardise calibrators — e.g., Cepheids or the tip of the red giant branch (TRGB); (ii) nearby Type Ia supernovae (hereafter SNe Ia) can be calibrated by standardised calibrators — e.g., Cepheids (Riess et al. 2021a, 2019; Dhawan et al. 2018; Riess et al. 2018b,a;

★ E-mail: dejaeger@hawaii.edu

Burns et al. 2018; Riess et al. 2016, 2011; Freedman & Madore 2010; Riess et al. 2009; Sandage et al. 2006; Freedman et al. 2001), TRGB (Dhawan et al. 2022; Freedman 2021; Anand et al. 2021; Yuan et al. 2019; Freedman et al. 2019; Jang & Lee 2017b,a; Madore et al. 2009), or Mira variable stars (Huang et al. 2020; Whitelock et al. 2008); and (iii) the calibration to nearby SNe Ia is applied to SNe Ia in the Hubble flow. Owing to a series of efforts which have allowed the scientific community to build the cosmic distance ladder over several decades, such as detached eclipsing binary stars in the Large Magellanic Cloud (Pietrzyński et al. 2019), *Gaia* parallaxes (Lindegren et al. 2021; Riess et al. 2021b), Cepheids (Leavitt & Pickering 1912), tip of the red giant branch (TRGB; Lee et al. 1993), and SNe Ia in the Hubble flow (SH0ES[1] team), the uncertainty in the local measurement of H_0 has improved from ~ 10% (Freedman et al. 2001) to ± 1.4% (Riess et al. 2021a) in the last twenty years. Using 42 SNe Ia calibrated with Cepheids, Riess et al. (2021a) have derived the most precise estimate of H_0 in the late Universe: $73.04 \pm 1.04\,\mathrm{km\,s^{-1}\,Mpc^{-1}}$. With the same technique but using 19 SNe Ia calibrated with TRGB, Freedman (2021) obtained $H_0 = 69.8 \pm 0.6$ (stat) ± 1.6 (sys) $\mathrm{km\,s^{-1}\,Mpc^{-1}}$. The difference between the TRGB and Cepheid calibrations is not yet understood (possible systematics in both methods), but it is not clear whether there is any significant difference between TRGB and Cepheid distances for SN Ia hosts. Riess et al. (2021b) compared the only 7 hosts in common and found no difference. Also, Anand et al. (2021) reanalysed the TRGB distances with different data to calibrate the zero-point in NGC 4258 and also found no significant difference with Cepheid results ($H_0 = 71.5 \pm 1.8\,\mathrm{km\,s^{-1}\,Mpc^{-1}}$). Moreover, Blakeslee et al. (2021) calibrated surface brightness fluctuations with Cepheids and TRGB, obtaining the same answer for each.

(ii) The alternate method is based on measurements of the early Universe using the sound horizon observed from the cosmic microwave background radiation (CMB; e.g., Planck Collaboration et al. 2018; Spergel et al. 2007; Bennett et al. 2003; Jaffe et al. 2001; Fixsen et al. 1996). However, unlike the distance-ladder technique, this method provides only an "inverse" cosmic distance ladder, calibrated at redshift $z \approx 1100$ and based on the physics of the early Universe extrapolated to $z \approx 0$. Assuming a Λ cold dark matter (ΛCDM) cosmological model, Planck Collaboration et al. (2018) derive a value of $H_0 = 67.4 \pm 0.5\,\mathrm{km\,s^{-1}\,Mpc^{-1}}$. Other works add an intermediate-redshift rung to anchor SNe Ia at $z > 0.1$ and find a consistent value (Macaulay et al. 2019). It is important to note that all the probes from the early Universe assume that the sound horizon calculation from the standard cosmological model is correct. For this reason, Baxter & Sherwin (2021) derive H_0 from the CMB without using information from the sound horizon scale. Their result, $H_0 = 73.5 \pm 5.3\,\mathrm{km\,s^{-1}\,Mpc^{-1}}$, is consistent with the local measurement but different from the Planck Collaboration et al. (2018) value.

The discrepancy between the two approaches, also referred to as the "H_0 tension," has reached a 5σ level of significance using Cepheids (Riess et al. 2021a) (though only a 1–2σ level of significance using TRGB Freedman 2021; Anand et al. 2021). This tension is difficult to explain by invoking systematic errors, because a multitude of independent methods have confirmed it. For example, Pesce et al. (2020) derived an independent H_0 value of $73.9 \pm 3.0\,\mathrm{km\,s^{-1}\,Mpc^{-1}}$ using geometric distance measurements to megamaser-hosting galaxies, and Blakeslee et al. (2021) obtained a value of $73.3 \pm 0.7 \pm 2.4\,\mathrm{km\,s^{-1}\,Mpc^{-1}}$ from surface brightness fluctuation distances for 63 bright early-type galaxies (see Di Valentino et al. 2021 for a review). To date, no solution has been found to explain the tension, but a wide variety of ideas have been proposed — e.g., the presence of additional species of neutrinos, early dark energy, decaying dark matter, or a breakdown of the general relativity (see Di Valentino et al. 2021 and Riess et al. 2021a for reviews).

In this work, as an independent approach to test the second and third rungs of the distance-ladder method (which rely on SNe Ia), we use Type II supernovae (SNe II; explosions of massive, evolved, hydrogen-envelope stars via core collapse). SNe II display a large range of peak luminosities, but can be calibrated via theoretical (Vogl 2020; Schmidt et al. 1994; Kirshner & Kwan 1974) and empirical methods (de Jaeger et al. 2020a; Rodríguez et al. 2019; de Jaeger et al. 2017b, 2015; Hamuy & Pinto 2002). Using the former, Schmidt et al. (1994) obtained an H_0 value of $73 \pm 13\,\mathrm{km\,s^{-1}\,Mpc^{-1}}$, while with the latter, values of $69 \pm 16\,\mathrm{km\,s^{-1}\,Mpc^{-1}}$ (standard candle method (SCM); Olivares E. et al. 2010) and $\sim 71 \pm 8\,\mathrm{km\,s^{-1}\,Mpc^{-1}}$ (photospheric magnitude method; Rodríguez et al. 2019) have been derived. More recently, by applying a refined version of the SCM (de Jaeger et al. 2020a) and using seven objects with Cepheid or TRGB independent host-galaxy distance measurements, de Jaeger et al. (2020b) demonstrated that SNe II also manifest the "H_0 tension" (albeit at a low level of significance). They found an H_0 value of $75.8^{+5.2}_{-4.9}\,\mathrm{km\,s^{-1}\,Mpc^{-1}}$ (stat) value, which differs by 1.4σ from the high-redshift result (Planck Collaboration et al. 2018). Finally, using a tailored-expanding-photosphere method (Vogl et al. 2019, 2020), Vogl (2020) obtain a value of $72.3 \pm 2.8\,\mathrm{km\,s^{-1}\,Mpc^{-1}}$, where again the uncertainties are only statistical. It is worth noting that the tailored-expanding-photosphere method is currently limited by a small sample size (only six objects) and peculiar-velocity corrections (mean $z = 0.02$), and it is affected by the systematic uncertainties of atmosphere models (Vogl et al. 2019; Dessart & Hillier 2005; Eastman et al. 1996). However, even if this method requires multiple well-calibrated spectra in the first month after the explosion, which is observationally expensive, it is a promising technique as it does not need calibrators. With this method, one can derive absolute SN II distances and therefore measure direct H_0 values without the risk of introducing systematic errors from the calibrators.

Here, as in de Jaeger et al. (2020b), we use the SCM to derive precise extragalactic distances, but importantly, we nearly double the number of calibrators (from 7 to 13). This allows us to derive H_0 with a precision of ~ 5% (statistical). Section 2 describes our methodology (data, calibrators, SCM), and we present our results in Section 3. Section 4 summarises our conclusions.

[1] "Supernovae, H_0 for the Equation of State of Dark Energy"; Riess et al. (2011).

2 METHOD

2.1 Data Sample

In this study, we consider the same SN II sample used by de Jaeger et al. (2020b), consisting of 125 objects (89 of which are at $z > 0.01$) from the following surveys: the Lick Observatory Supernova Survey (LOSS; Filippenko et al. 2001), the Carnegie Supernova Project-I (CSP-I; Hamuy et al. 2006), the Sloan Digital Sky Survey-II SN Survey (SDSS-II; Frieman et al. 2008), the Supernova Legacy Survey (SNLS; Astier et al. 2006), the Subaru Hyper-Suprime Cam Survey (SSP-HSC; Aihara et al. 2018; Miyazaki et al. 2012), and the Dark Energy Survey Supernova Program (DES-SN; Bernstein et al. 2012). To this sample we also add four SNe II for which we have absolute SN host distance measurements: SN 2014bc (Polshaw et al. 2015), SN 2017eaw (Van Dyk et al. 2019), SN 2018aoq (unpublished Lick/KAIT data), and SN 2020yyz (unpublished *Hubble Space Telescope* data and public Zwicky Transient Factory data; Bellm et al. 2019). We refer the reader to de Jaeger et al. (2020b) and references therein for more detailed information regarding the surveys, photometric reduction, and how the magnitudes are simultaneously corrected for Milky Way extinction, K-corrected, and S-corrected. Note that as in de Jaeger et al. (2020b), all of the CMB redshifts ($z_{\rm CMB}$) are taken from the NASA/IPAC Extragalactic Database (NED[2]). Then, to account for peculiar velocities, all are corrected (henceforth referred to as $z_{\rm corr}$) using the model of Carrick et al. (2015). Finally, a residual peculiar-velocity uncertainty of 250 km s^{-1} is added to the total redshift uncertainty in quadrature.

2.2 Calibrator sample

This work uses 13 SNe II having absolute distance measurements: one with a geometric distance, seven with Cepheid-derived distances, and five from the TRGB. Among these calibrators, seven were already used (and thus described) by de Jaeger et al. (2020b). We list the remaining six below.

- SN 2004et and SN 2017eaw in NGC 6946: de Jaeger et al. (2020b) did not include these objects because they had a large Milky Way extinction, and at that time, the TRGB distance was not reliable (only a few stars). In this work, we add both objects because the colour-magnitude diagram from the Extragalactic Distance Database (EDD[3]) is now well sampled. This means that unlike in Anand et al. (2018), the break in the stellar luminosity function is now sharper and therefore more reliable. To consider the large Milky Way extinction, we account for it in the distance error by adding 10% of the extinction (0.1 mag) in quadrature. The final distance modulus used is $\mu = 29.21 \pm 0.16$ mag.
- SN 2008bk in NGC 7793: This SN was also removed from de Jaeger et al. (2020b) because its distance was obtained using ground-based observations with only 11 Cepheids. However, a TRGB measurement (Anand et al. 2021) is now available in the EDD. The distance modulus used in this work is $\mu = 27.80 \pm 0.08$ mag.
- SN 2014bc ($\mu = 29.387 \pm 0.0568$ mag; Reid et al. 2019) in NGC 4258 using the Keplerian motion of masers.
- SN 2018aoq ($\mu = 31.04 \pm 0.07$ mag; Yuan et al. 2020) in NGC 4151 using Cepheids.
- SN 2020yyz ($\mu = 31.71 \pm 0.157$ mag; Riess et al. 2021a) in NGC 0976 using Cepheids.

The TRGB luminosities are converted into distance moduli using a zero-point calibration of −4.01, which is the average of many recent measurements as compiled by Li et al. (2022, see their Table 3) and an uncertainty of 0.04 mag. Additionally, the Cepheid distances have been revised and updated from Riess et al. (2021a). It is important to note that because it is not clear whether there is any significant difference between TRGB and Cepheid distances for SN Ia hosts (see Sec. 1), here we use TRGB and Cepheid distance measurements together to increase the total number of calibrators and decrease the statistical error in H_0. Also, in Section 3.1, we show that the mean SN II luminosity from TRGB and Cepheids is consistent (differing by $\sim 0.3\sigma$), which supports the use of both calibrators together. A summary of all the calibrators available in this work and their distances can be found in Table 1.

2.3 Empirical SN II standardisation

SNe II are not standard candles, but they are standardisable using theoretical or empirical methods. Here, we follow the methodology of de Jaeger et al. (2020b) and use the SCM, which leverages the correlation between SN II luminosity and two observables: (i) the photospheric expansion velocity, and (ii) colour. Intrinsically brighter SNe II have more-rapidly expanding photospheres and are bluer (see Figures 7 and 8 of de Jaeger et al. 2020a). Therefore, for each SN, the corrected magnitude is written as

$$m_{\rm corr} = {\rm m} + \alpha \log_{10}\left(\frac{v_{{\rm H}\beta}}{\bar{v}_{{\rm H}\beta}}\right) - \beta(c - \bar{c}) \,, \quad (1)$$

where m is the apparent magnitude in a given passband at 43 d after the explosion, c is the colour, $v_{{\rm H}\beta}$ is the velocity measured using Hβ absorption from an optical spectrum, and the overbars are used to denote averaged quantities. The nuisance parameters α and β are discussed below. For more details, we refer the reader to Equations (1), (2), and (3) of de Jaeger et al. (2020a).

2.4 H_0 from SNe II

This section describes how H_0 can be derived from SNe II using the SCM. As the methodology is the same as that used by de Jaeger et al. (2020a), only a brief description is presented here.

As defined by Riess et al. (2011),

$$\log_{10}\ {\rm H}_0 = \frac{M_i + 5\,a_i + 25}{5}, \quad (2)$$

where a_i is the intercept of the SN II magnitude-redshift relation (translated to $z = 0$) measured from the Hubble-flow sample and M_i is the absolute SN II i-band magnitude (at 43 d) derived using our calibrator sample. Therefore, the approach is to fit a joint model which combines the calibrator

[2] http://ned.ipac.caltech.edu/
[3] https://edd.ifa.hawaii.edu/

Table 1. Calibrator sample.

SN name	Host Galaxy	μ (mag)	calibrator	references
SN 1999em	NGC 1637	30.26 ± 0.09	Cepheids	de Jaeger et al. (2020b) (updated from Leonard et al. 2003)
SN 1999gi	NGC 3184	30.64 ± 0.11	Cepheids	de Jaeger et al. (2020b) (updated from Leonard et al. 2002)
SN 2004et	NGC 6946	29.21 ± 0.16	TRGB	From EDD, Anand et al. (2021)
SN 2005ay	NGC 3938	31.72 ± 0.07	Cepheids	Riess et al. (2021a)
SN 2005cs	NGC 5194/M51	29.62 ± 0.09	TRGB	de Jaeger et al. (2020b) (updated from McQuinn et al. 2017)
SN 2008bk	NGC 7793	27.80 ± 0.08	TRGB	From EDD, Anand et al. (2021)
SN 2009ib	NGC 1559	31.49 ± 0.06	Cepheids	Riess et al. (2021a)
SN 2012aw	NGC 3351	29.82 ± 0.09	Cepheids	de Jaeger et al. (2020b) (updated from Kanbur et al. (2003))
SN 2013ej	NGC 628/M74	29.90 ± 0.08	TRGB	de Jaeger et al. (2020b) (updated from McQuinn et al. (2017))
SN 2014bc	NGC 4258	29.387 ± 0.0568	Geometric	Reid et al. (2019)
SN 2017eaw	NGC 6946	29.21 ± 0.16	TRGB	From EDD, Anand et al. (2021)
SN 2018aoq	NGC 4151	31.04 ± 0.07	Cepheids	Yuan et al. (2020)
SN 2020yyz	NGC 0976	31.71 ± 0.15	Cepheids	Riess et al. (2021a)

and Hubble-flow samples to constrain M_i and to determine a_i. Simultaneously, our model evaluates how close the calibrators are to the mean absolute magnitude, and, given a value of H_0, how close the absolute magnitudes of the Hubble-flow SNe II are to the mean absolute magnitude.

However, as the SNe II are not standard candles, we also need to standardise their apparent magnitudes by deriving α and β from Equation 1. Our model thus has five free parameters: α, β, H_0, M_i, and $\sigma_{\rm int}$, where $\sigma_{\rm int}$ is the usual uncertainty added to account for unmodelled, intrinsic SN II scatter. As in de Jaeger et al. (2020a), we use the Python package EMCEE developed by Foreman-Mackey et al. (2013) with 300 walkers, 2000 steps, and with uniform priors for α, $\beta \neq 0$, $H_0 > 0$, and $M_i < 0$, and scale-free for $\sigma_{\rm int} > 0$ with $p(\sigma_{\rm int}) = 1/\sigma_{\rm int}$.

3 RESULTS

3.1 Calibrators

Following de Jaeger et al. (2020a), who demonstrated that the best passband to minimise the intrinsic dispersion among SNe II in the Hubble diagram is the i band, we use the same band and show, in Figure 1, the absolute magnitudes of all 13 calibrators. The calibrators have a weighted average absolute magnitude of −16.71 mag, with a dispersion of $\sigma_{\rm cal} = 0.29$ mag — similar to those obtained by de Jaeger et al. (2020a) (−16.69 mag and 0.24 mag, respectively) and as expected, larger in scatter than that obtained using SNe Ia and 42 calibrators (0.13 mag; Riess et al. 2021a). Although the method to standardise SNe II is not as strong as the one used for SNe Ia, the dispersion increases to 0.80 mag when the SCM is not applied, demonstrating its utility.

It is interesting to compare the average absolute magnitude obtained for both types of calibrators. For our 5 TRGBs, we find an average absolute magnitude of −16.81 ± 0.33 mag, while for our 7 Cepheids −16.68 ± 0.25 mag. The absolute magnitude for the TRGB is slightly larger than, but fully consistent with, the Cepheids. Small-number statistics may explain the difference, as in de Jaeger et al. (2020a) the difference was ∼ 1σ with two TRGBs and five Cepheids, while in this work it is just ∼ 0.3σ.

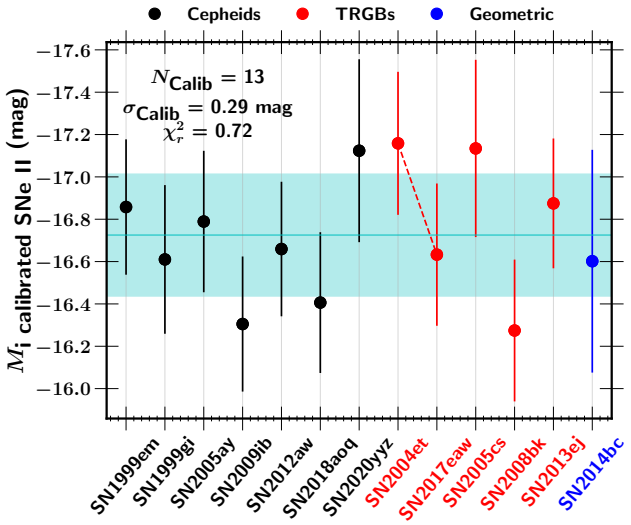

Figure 1. Absolute i-band magnitude 43 d after the explosion for the 13 calibrators based on Cepheid (black), TRGB (red), or geometric (blue) distances. We also present the standard deviation obtained after applying the SCM, represent it by the cyan filled region. A dashed line connecting SN 2004et and SN 2017eaw has been plotted to indicate that they are located in the same host galaxy. Note that the uncertainties include the intrinsic scatter ($\sigma_{\rm int} = 0.29$ mag) as well as the reduced χ^2_r.

3.2 Hubble-Lemaître constant

To minimise the effect of peculiar velocities we select only SNe II with $z_{\rm corr} > 0.01$ in our Hubble-flow sample ($N = 89$). With the 13 calibrators described in Section 2.2, we obtain a median value of $H_0 = 75.4^{+3.8}_{-3.7}$ km s^{-1} Mpc^{-1}, where the quoted uncertainties are statistical only. This value is consistent with the one derived by de Jaeger et al. (2020b) with seven calibrators ($H_0 = 75.8^{+5.2}_{-4.9}$ km s^{-1} Mpc^{-1}); however, with the addition of six calibrators, we reduce the statistical uncertainty by 25% (5.0% vs. 6.7%; see de Jaeger et al. 2020b). As expected and seen in Figure 2, the other free-fitting parameters (α, β, M_i, and $\sigma_{\rm int}$) are only slightly different with respect to de Jaeger et al. (2020b), as we use the

same Hubble-flow sample and add six new nearby objects. Note that the intrinsic scatter derived for the SNe II in the Hubble flow and the nearby SNe II is consistent (0.28 mag vs. 0.29 mag).

Regarding the "H_0 tension," our result is consistent with the local measurement from SNe Ia ($73.04 \pm 1.04\,\mathrm{km\,s^{-1}\,Mpc^{-1}}$; Riess et al. 2021a), and shows a discrepancy of 2.2σ with the early-Universe value ($H_0 = 67.4 \pm 0.5\,\mathrm{km\,s^{-1}\,Mpc^{-1}}$; Planck Collaboration et al. 2018). If we use only the Cepheids to measure H_0 ($N = 7$), we obtain $H_0 = 77.6^{+5.2}_{-4.8}\,\mathrm{km\,s^{-1}\,Mpc^{-1}}$, while using only TRGB ($N = 5$), we find $H_0 = 73.1^{+5.7}_{-5.3}\,\mathrm{km\,s^{-1}\,Mpc^{-1}}$. There is no meaningful difference between our results derived from TRGB or from Cepheids.

A summary of our data, H_0 fit, and residuals is shown in Figure 3, where we see only the second and third rungs of the distance-ladder method that have been tested in this work. The second rung allows us to calibrate and derive the SN II absolute i-band magnitude using 13 calibrators (geometric, Cepheids, TRGB), while the third rung uses SNe II in the Hubble flow to constrain H_0.

3.3 Systematic uncertainties

In this section, we investigate possible sources of systematic errors in our measurement. For this, we look at the effect of different cuts and calibrators on H_0. We summarise all the results in Table 2.

First, because peculiar velocities can systematically affect H_0 measurements (Boruah et al. 2021; Sedgwick et al. 2021), we investigate what changes in the associated uncertainty in the recession velocities have on our determination of H_0. We find that changing the error to $150\,\mathrm{km\,s^{-1}}$ instead of $250\,\mathrm{km\,s^{-1}}$ only changes the value by 0.2% ($75.3^{+4.0}_{-3.7}\,\mathrm{km\,s^{-1}\,Mpc^{-1}}$). Then, we investigate what changes if we cut our Hubble-flow sample at $z_{\mathrm{corr}} > 0.023$ (Riess et al. 2021a). With this cut, our Hubble-flow sample decreases to 47 SNe II and we find a value of $77.6^{+4.7}_{-4.5}\,\mathrm{km\,s^{-1}\,Mpc^{-1}}$ — an increase of 2.9% with respect to our fiducial model. If we apply a less-restrictive redshift cut and use all the SNe II ($z_{\mathrm{corr}} > 0.0$), a decrease of 1.3% is seen ($H_0 = 74.4^{+3.7}_{-3.3}\,\mathrm{km\,s^{-1}\,Mpc^{-1}}$). Finally, we investigate what changes if we use uncorrected CMB-frame redshifts rather than redshifts corrected for peculiar velocities. In this case, H_0 decreases by 0.5% to $75.0^{+3.8}_{-3.6}\,\mathrm{km\,s^{-1}\,Mpc^{-1}}$. The effect on H_0 seen when applying different redshift cuts can be explained by peculiar velocities that are not perfectly corrected or by small-number statistics of the Hubble-flow sample (the largest difference is seen when the sample is reduced to 47 objects).

Second, we investigate the effect of the calibrators on H_0. Using only Cepheids or TRBGs as calibrators causes the largest differences relative to the fiducial model. We find a difference of 2.9% ($77.6^{+5.2}_{-4.8}\,\mathrm{km\,s^{-1}\,Mpc^{-1}}$) and 3% ($73.1^{+5.7}_{-5.6}\,\mathrm{km\,s^{-1}\,Mpc^{-1}}$) with only Cepheids and only TRGBs, respectively. The small discrepancy between the TRGB and Cepheid values could hint that there might be a systematic difference between the TRGB and Cepheid methods, as possibly seen with SNe Ia (see Riess et al. 2021b; Freedman 2021; Anand et al. 2021). However, our TRGB and Cepheid values are consistent, differing by $< 1.0\sigma$. Also, both values are in the range of other local measures (Di Valentino et al. 2021) and statistically inconsistent with the *Planck*+ΛCDM value, suggesting that neither points to the source of the tension.

Finally, two SNe II (SN 2004et and SN 2017eaw) with TRGB distance measurements have a large Milky Way extinction. If we remove them from our calibrator sample, H_0 increases to $77.0^{+4.4}_{-4.3}\,\mathrm{km\,s^{-1}\,Mpc^{-1}}$ (difference of 2.2%). We expect to find a higher value than in our fiducial model because after removing two TRGB distance measurements, the Cepheid calibrator sample size represents ~ 63% (vs. ~ 53%) of all the calibrators. As the Cepheid H_0 value is larger than the TRGB H_0 value, our H_0 value excluding those two SNe II from the TRGB sample will move toward a higher value than our fiducial model.

Finally, we investigate the effect of the different surveys. Using only the CSP-I sample or removing it only affects our fiducial H_0 measurement by 0.5%. The major differences are seen when only the low-z KAIT sample is used or removed, producing a difference of 3.0% and 1.2%, respectively. The largest difference could be explained by a small number of SNe II in the Hubble flow (19) or by intrinsic SN II differences. However, no significant differences are seen in the magnitude, velocity, and colour distributions of the CSP-I and KAIT surveys. Finally, excluding the two low-z samples (CSP-I and KAIT) increases the H_0 value to $77.2^{+4.8}_{-4.4}\,\mathrm{km\,s^{-1}\,Mpc^{-1}}$, a difference of 2.4%.

All 13 H_0 measurements from the aforementioned analysis variants are consistent with our fiducial model. The median and standard deviation of all the variants are $75.1 \pm 1.5\,\mathrm{km\,s^{-1}\,Mpc^{-1}}$, which corresponds to only $0.3\,\mathrm{km\,s^{-1}\,Mpc^{-1}}$ lower than our fiducial value (only ~ 8% of the statistical uncertainty). Following the conservative approach of Riess et al. (2019), our systematic uncertainty is calculated as the standard deviation of our variants. From the 13 variants presented in Table 2, we obtain a systematic uncertainty of $\sim 1.5\,\mathrm{km\,s^{-1}\,Mpc^{-1}}$ (~ 2%). Including both statistical and systematic uncertainties, our H_0 value is $75.4^{+3.8\ (\mathrm{stat})}_{-3.7\ (\mathrm{stat})} \pm 1.5\ (\mathrm{sys})\,\mathrm{km\,s^{-1}\,Mpc^{-1}}$. This is the most precise H_0 value obtained from SNe II with the SCM. Taking into account both sources of uncertainties, our value differs by 2.0σ from the high-redshift results (Planck Collaboration et al. 2018) and by only 0.6σ from the local measurement (Riess et al. 2021a).

3.4 Bootstrap simulation

We perform a bootstrap resampling of the set of calibrators, with replacement (see Figure 4), to study the calibrator effects on H_0. With 13 calibrators, we explore a total of 5,200,300 possibilities (25!/13!12!) and obtain a median value of $75.5 \pm 3.7\,\mathrm{km\,s^{-1}\,Mpc^{-1}}$. The peak of the distribution is consistent with the original value and the local measurements using SNe Ia (Riess et al. 2021a), but almost does not overlap with the *Planck*+ΛCDM value. Only 1.4% of the 5,200,300 H_0 samples are smaller than $67.9\,\mathrm{km\,s^{-1}\,Mpc^{-1}}$, which corresponds to *Planck*+ΛCDM value $+1\sigma$. Finally, as in de Jaeger et al. (2020b), our distribution also extends to large H_0 values (85–$95\,\mathrm{km\,s^{-1}\,Mpc^{-1}}$), and this behaviour is driven by the faintest calibrators (SN 2009ib, SN 2018aoq, and SN 2008bk).

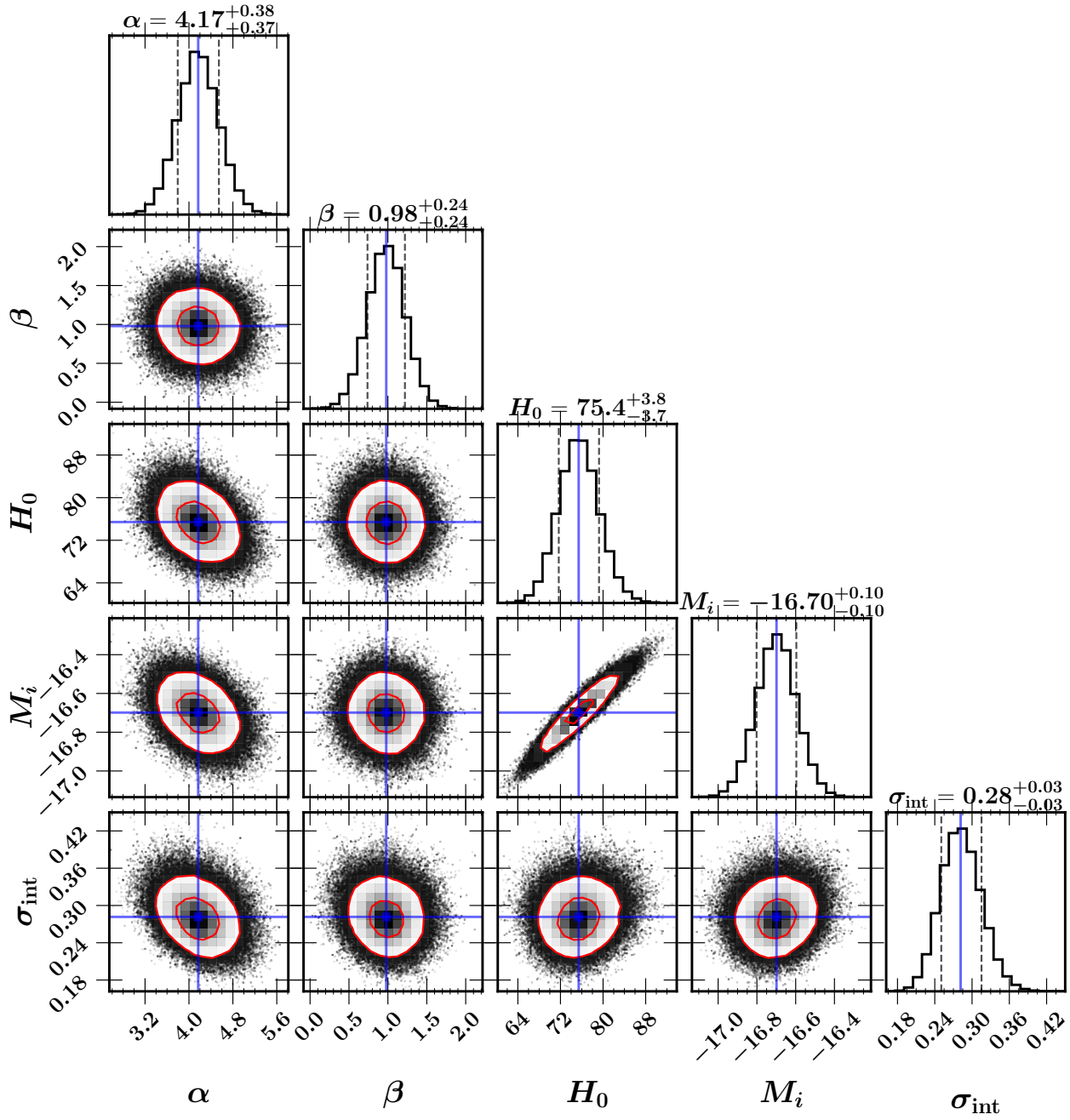

Figure 2. Corner plot showing all one- and two-dimensional projections of our fitted parameters: α, β, H_0, M_i, and $\sigma_{\rm int}$. Data points shown in grey and red contours are given at 1σ and 2σ (which corresponds in two dimensions to the 39% and 86% of the volume). For each parameter, the median value and the 16th and 84th percentile differences are shown.

4 CONCLUSIONS

In this work, we test the second and the third rungs of the SN Ia distance ladder. For this purpose, we use SNe II to provide an independent measurement of H_0. With 13 objects having geometric, Cepheid, or TRGB host-galaxy distance measurements, we derive $H_0 = 75.4^{+3.8}_{-3.7}$ km s^{-1} Mpc^{-1}, where the quoted uncertainties are statistical only.

By analysing 13 variants to our fiducial model, we also investigate the possible sources of systematic error. We find that all 13 H_0 measurements are consistent with our fiducial model, and the median value only differs by 0.3 km s^{-1} Mpc^{-1}. From our 13 variants, we obtain a standard deviation of ~ 1.5 km s^{-1} Mpc^{-1} ($\sim 2\%$), which we interpret as an estimate of the systematic error in the SCM. Combining systematic and statistical uncertainties, we derive a value of $75.4^{+3.8}_{-3.7}$ (stat) ± 1.5 (sys) km s^{-1} Mpc^{-1}. Our value is consistent with the local measurement (Riess et al. 2021a) and differs by 2.0σ from the high-redshift results (Planck Collaboration et al. 2018). Therefore, this demonstrates that there is no evidence that SNe Ia are the source of the "H_0 tension"; the third rung of the cosmic distance ladder, yielded by SNe Ia and SNe II, is consistent.

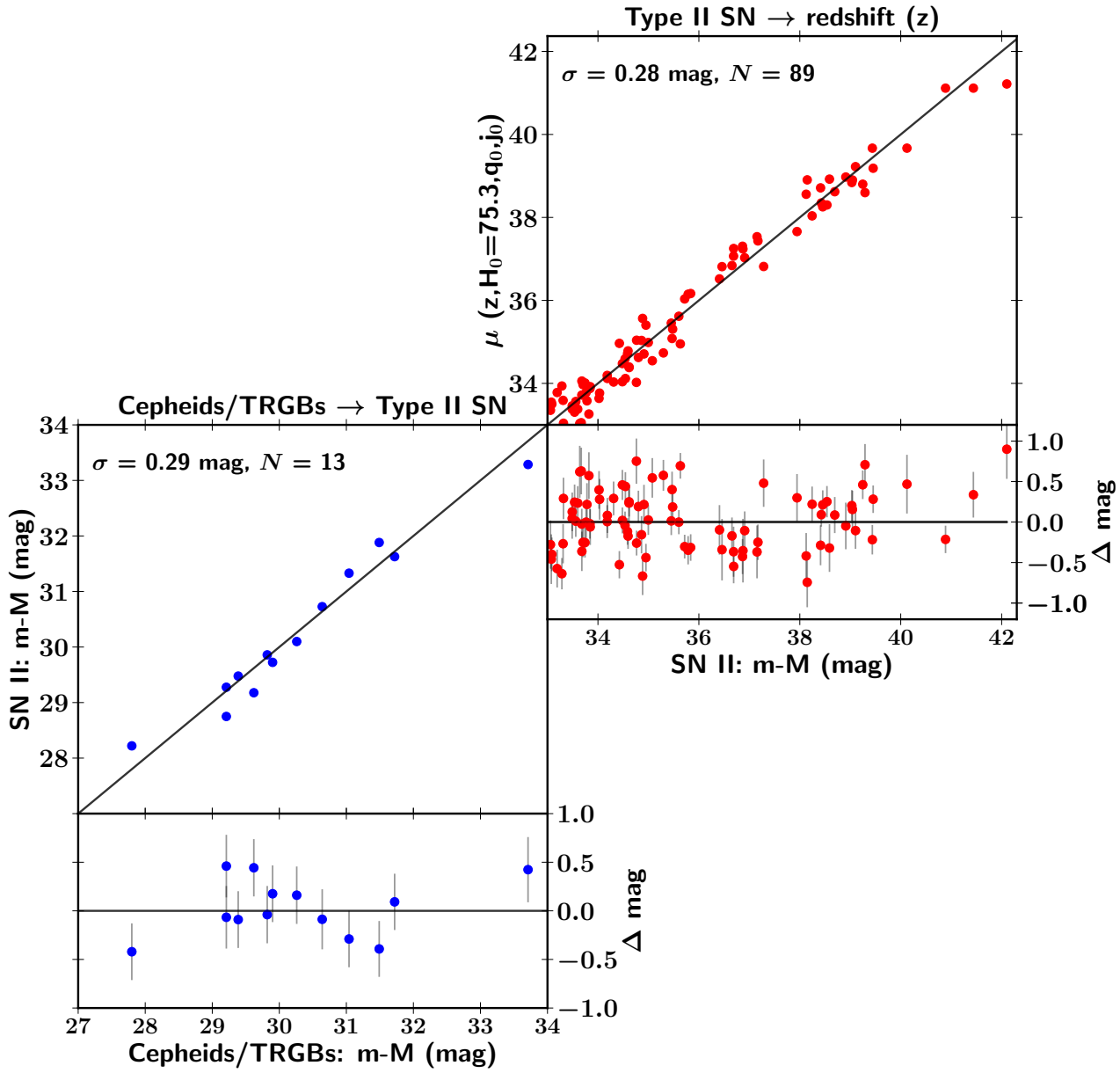

Figure 3. Figure similar to the SNe Ia figure of Riess et al. (2021a), representing the last two rungs of the distance ladder: Cepheid- and SN-based (bottom left), and SN- and redshift-based (top right). Blue dots represents the SNe II with geometric, Cepheid, or TRGB distances to estimate M_i. Red dots are the SNe II in the Hubble flow used to derive H_0.

We also perform a bootstrap simulation to study the calibrator effects on H_0. The peak of our distribution is consistent with the local measurements using SNe Ia (Riess et al. 2021a) but almost does not overlap with the *Planck*+ΛCDM value. Only 1.4% of the 5,200,300 H_0 values are smaller than 67.9 km s^{-1} Mpc^{-1} which corresponds to the *Planck*+ΛCDM value +1σ.

Finally, with the availability of two sources of calibration, Cepheids or TRGB, we investigate the role of either in the "H_0 tension." With seven Cepheids or five TRGB, we derive consistent values which differ by < 1.0σ (difference of 4.5 km s^{-1} Mpc^{-1} between Cepheids and TRGB). Both values are also in the range of several other local measures (Di Valentino et al. 2021). Thus, despite the larger uncertainties of our values, we find no indication of Cepheids or TRGB as the source of the "H_0 tension." This is in good agreement with the results from Blakeslee et al. (2021), Kourkchi et al. (2022), Anand et al. (2021), and Riess et al. (2021a), who found no significant difference in H_0 between the use of Cepheids and TRGB.

With upcoming studies, we will increase the number of SNe II in the Hubble flow and reduce the systematic uncertainties due to peculiar velocities. Also, as shown in this paper, with a larger number of calibrators, we will be able to reduce our statistical uncertainty. Finally, having more Cepheid and TRGB distance measurements will allow us to better test the second rung of the distance ladder and see

Table 2. Free-parameter values for different sample choices.

Sample	Cali	$N_{\rm cali}$	$\sigma_{\rm cali}$ (mag)	$N_{\rm SNe}$	α	β	H_0 (km s^{-1} Mpc^{-1})	M_i (mag)	$-5\,a_i$ (mag)	$\sigma_{\rm int}$ (mag)	ΔH_0
Fiducial	C+T+G	13	0.29	89	$4.17^{+0.38}_{-0.37}$	$0.98^{+0.24}_{-0.24}$	$75.4^{+3.8}_{-3.7}$	$-16.70^{+0.10}_{-0.10}$	$-1.09^{+0.04}_{-0.04}$	$0.28^{+0.03}_{-0.03}$	...
Peculiar-Velocity Variants											
$v_{\rm pec}$ = 150	C+T+G	13	0.29	89	$4.15^{+0.38}_{-0.36}$	$0.98^{+0.24}_{-0.25}$	$75.3^{+4.0}_{-3.7}$	$-16.70^{+0.10}_{-0.10}$	$-1.08^{+0.04}_{-0.04}$	$0.29^{+0.03}_{-0.03}$	0.2%
$z_{\rm cmb}$	C+T+G	13	0.29	89	$4.11^{+0.37}_{-0.37}$	$1.04^{+0.25}_{-0.24}$	$75.0^{+3.8}_{-3.6}$	$-16.70^{+0.10}_{-0.10}$	$-1.08^{+0.04}_{-0.04}$	$0.28^{+0.03}_{-0.03}$	0.5%
$z_{\rm corr} > 0.023$	C+T+G	13	0.29	47	$4.36^{+0.53}_{-0.51}$	$0.57^{+0.35}_{-0.34}$	$77.6^{+4.7}_{-4.5}$	$-16.80^{+0.12}_{-0.12}$	$-1.25^{+0.05}_{-0.05}$	$0.28^{+0.04}_{-0.04}$	2.9%
$z_{\rm corr} > 0.0$	C+T+G	13	0.29	116	$4.24^{+0.34}_{-0.34}$	$1.08^{+0.23}_{-0.23}$	$74.4^{+3.7}_{-3.4}$	$-16.64^{+0.10}_{-0.10}$	$-1.00^{+0.03}_{-0.03}$	$0.27^{+0.03}_{-0.03}$	1.3%
Calibrator Sample Variants											
$z_{\rm corr} > 0.01$	C	7	0.24	89	$4.12^{+0.44}_{-0.43}$	$0.88^{+0.25}_{-0.24}$	$77.6^{+5.2}_{-4.8}$	$-16.64^{+0.13}_{-0.13}$	$-1.09^{+0.04}_{-0.04}$	$0.28^{+0.03}_{-0.03}$	2.9%
$z_{\rm corr} > 0.01$	T	5	0.33	89	$4.07^{+0.40}_{-0.40}$	$1.04^{+0.28}_{-0.28}$	$73.1^{+5.7}_{-5.3}$	$-16.77^{+0.16}_{-0.16}$	$-1.09^{+0.04}_{-0.04}$	$0.29^{+0.03}_{-0.03}$	3.0%
$-$04et, 17eaw	C+T+G	11	0.28	89	$4.11^{+0.39}_{-0.38}$	$0.92^{+0.24}_{-0.25}$	$77.0^{+4.4}_{-4.3}$	$-16.65^{+0.12}_{-0.12}$	$-1.09^{+0.04}_{-0.04}$	$0.28^{+0.03}_{-0.03}$	2.2%
Hubble-Flow Sample Variants											
Only CSP-I	C+T+G	13	0.29	37	$4.20^{+0.48}_{-0.47}$	$0.98^{+0.32}_{-0.31}$	$75.1^{+4.1}_{-3.9}$	$-16.65^{+0.10}_{-0.10}$	$-1.02^{+0.05}_{-0.05}$	$0.27^{+0.04}_{-0.04}$	0.5%
No CSP-I	C+T+G	13	0.29	52	$4.33^{+0.49}_{-0.48}$	$0.96^{+0.31}_{-0.31}$	$75.0^{+4.4}_{-4.1}$	$-16.75^{+0.11}_{-0.11}$	$-1.13^{+0.05}_{-0.05}$	$0.28^{+0.05}_{-0.05}$	0.5%
Only KAIT	C+T+G	13	0.32	19	$4.87^{+0.69}_{-0.67}$	$1.29^{+0.40}_{-0.39}$	$73.2^{+4.6}_{-4.5}$	$-16.66^{+0.11}_{-0.10}$	$-0.98^{+0.09}_{-0.08}$	$0.26^{+0.09}_{-0.13}$	3.0%
No KAIT	C+T+G	13	0.29	70	$4.00^{+0.40}_{-0.38}$	$0.83^{+0.26}_{-0.26}$	$76.3^{+4.0}_{-3.8}$	$-16.70^{+0.10}_{-0.10}$	$-1.11^{+0.04}_{-0.04}$	$0.27^{+0.03}_{-0.03}$	1.2%
CSP-I+KAIT	C+T+G	13	0.29	56	$4.36^{+0.43}_{-0.43}$	$1.14^{+0.28}_{-0.28}$	$74.4^{+4.1}_{-3.9}$	$-16.65^{+0.10}_{-0.11}$	$-1.01^{+0.05}_{-0.05}$	$0.28^{+0.04}_{-0.04}$	1.3%
"high-z"	C+T+G	13	0.29	33	$4.11^{+0.53}_{-0.52}$	$0.68^{+0.35}_{-0.35}$	$77.2^{+4.8}_{-4.4}$	$-16.78^{+0.12}_{-0.11}$	$-1.22^{+0.06}_{-0.06}$	$0.26^{+0.05}_{-0.05}$	2.4%

Effect of systematic errors on the best-fitting values using the SCM and different samples. The fiducial line corresponds to the values obtained in Section 3.2, i.e., $z_{\rm corr} > 0.01$, 13 calibrators, and 89 SNe II in the Hubble flow. We try different cuts in redshift ($z_{\rm corr}$), surveys (e.g., only/no CSP-I, only/no KAIT, only CSP-I+KAIT, only high-z), calibrators [Cepheids (C) and/or TRGBs (T) and/or geometric (G)], and also remove some calibrators (e.g., $-$04et and $-$17eaw for SN 2004et and SN 2017eaw). The median value with the 16th and 84th percentile differences for each parameter are given together with their statistical uncertainties. The last column, ΔH_0, corresponds to the percentage difference from the fiducial model.

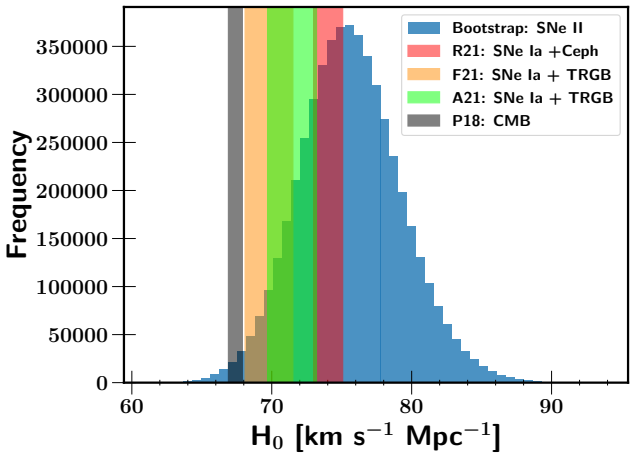

Figure 4. Histogram of our bootstrap resampling of the set of calibrators, with replacement. This histogram consists of 51 bins and contains a total of 5,200,300 simulations. An average value of 75.5±3.7 km s^{-1} Mpc^{-1} is derived. The red, orange, lime, and black filled regions correspond to the H_0 values obtained (respectively) by Riess et al. (2021a), Freedman (2021), Anand et al. (2021), and Planck Collaboration et al. (2018). Only 1.4% of the 5,200,300 H_0 values are smaller than 67.4 + 0.5 km s^{-1} Mpc^{-1} (Planck Collaboration et al. 2018).

whether there is a systematic difference between both calibrators.

ACKNOWLEDGEMENTS

We thank the referee for their comments on the manuscript, which helped improve it. Support for T.d.J. has been provided by U.S. NSF grants AST-1908952 and AST-1911074. L.G. acknowledges financial support from the Spanish Ministerio de Ciencia e Innovación (MCIN), the Agencia Estatal de Investigación (AEI) 10.13039/501100011033, and the European Social Fund (ESF) "Investing in your future" under the 2019 Ramón y Cajal program RYC2019-027683-I and the PID2020-115253GA-I00 HOSTFLOWS project, from Centro Superior de Investigaciones Científicas (CSIC) under the PIE project 20215AT016, and the program Unidad de Excelencia María de Maeztu CEX2020-001058-M. Support for A.V.F.'s supernova research at U.C. Berkeley has been provided by the NSF through grant AST-1211916, the TABASGO Foundation, Gary and Cynthia Bengier, Marc J. Staley (whose fellowship partially funded B.E.S. whilst contributing to the work presented herein as a graduate student), the Christopher R. Redlich Fund, the Sylvia and Jim Katzman Foundation, and the Miller Institute for Basic Research in Science (A.V.F. was a Miller Senior Fellow). B.J.S. is supported by U.S. NSF grants AST-1907570, AST-1908952, AST-1920392, and AST-1911074. The work of the CSP-I has been supported by the U.S. NSF under grants AST-0306969, AST-0607438, and AST-1008343.

KAIT and its ongoing operation were made possible by donations from Sun Microsystems, Inc., the Hewlett-Packard Company, AutoScope Corporation, Lick Observatory, the U.S. NSF, the University of California, the Sylvia & Jim Katzman Foundation, and the TABASGO Foundation. Research at Lick Observatory is partially supported by a generous gift from Google. This research used the Savio computational cluster resource provided by the Berkeley Re-

search Computing program at U.C. Berkeley (supported by the U.C. Berkeley Chancellor, Vice Chancellor for Research, and Chief Information Officer).

This paper is based in part on data collected at the Subaru Telescope and retrieved from the HSC data archive system, which is operated by the Subaru Telescope and Astronomy Data Center at the National Astronomical Observatory of Japan (NAOJ). The Hyper Suprime-Cam (HSC) collaboration includes the astronomical communities of Japan and Taiwan, and Princeton University. The HSC instrumentation and software were developed by the NAOJ, the Kavli Institute for the Physics and Mathematics of the Universe (Kavli IPMU), the University of Tokyo, the High Energy Accelerator Research Organization (KEK), the Academia Sinica Institute for Astronomy and Astrophysics in Taiwan (ASIAA), and Princeton University. Funding was contributed by the FIRST program from the Japanese Cabinet Office, the Ministry of Education, Culture, Sports, Science and Technology (MEXT), the Japan Society for the Promotion of Science (JSPS), the Japan Science and Technology Agency (JST), the Toray Science Foundation, NAOJ, Kavli IPMU, KEK, ASIAA, and Princeton University.

The Pan-STARRS1 Surveys (PS1) were made possible through contributions of the Institute for Astronomy, the University of Hawaii, the Pan-STARRS Project Office, the Max-Planck Society and its participating institutes, the Max Planck Institute for Astronomy, Heidelberg and the Max Planck Institute for Extraterrestrial Physics, Garching, The Johns Hopkins University, Durham University, the University of Edinburgh, Queen's University Belfast, the Harvard-Smithsonian Center for Astrophysics, the Las Cumbres Observatory Global Telescope Network Incorporated, the National Central University of Taiwan, the Space Telescope Science Institute, the National Aeronautics and Space Administration (NASA) under grant No. NNX08AR22G issued through the Planetary Science Division of the NASA Science Mission Directorate, the U.S. NSF under grant AST-1238877, the University of Maryland, and Eotvos Lorand University (ELTE). This paper makes use of software developed for the Large Synoptic Survey Telescope. We thank the LSST Project for making their code available as free software at http://dm.lsst.org.

Some of the data presented herein were obtained at the W. M. Keck Observatory, which is operated as a scientific partnership among the California Institute of Technology, the University of California, and NASA; the observatory was made possible by the generous financial support of the W. M. Keck Foundation. This work is based in part on data produced at the Canadian Astronomy Data Centre as part of the CFHT Legacy Survey, a collaborative project of the National Research Council of Canada and the French Centre National de la Recherche Scientifique. The work is also based on observations obtained at the Gemini Observatory, which is operated by the Association of Universities for Research in Astronomy, Inc., under a cooperative agreement with the U.S. NSF on behalf of the Gemini partnership: the U.S. NSF, the STFC (United Kingdom), the National Research Council (Canada), CONICYT (Chile), the Australian Research Council (Australia), CNPq (Brazil), and CONICET (Argentina). This research used observations from Gemini program numbers GN-2005A-Q-11, GN-2005B-Q-7, GN-2006A-Q-7, GS-2005A-Q-11, GS-2005B-Q-6, and GS-2008B-Q-56. This research has made use of the NASA/IPAC Extragalactic Database (NED), which is operated by the Jet Propulsion Laboratory, California Institute of Technology, under contract with NASA, and of data provided by the Central Bureau for Astronomical Telegrams.

Funding for the DES Projects has been provided by the U.S. Department of Energy, the U.S. NSF, the Ministry of Science and Education of Spain, the Science and Technology Facilities Council of the United Kingdom, the Higher Education Funding Council for England, the National Center for Supercomputing Applications at the University of Illinois at Urbana-Champaign, the Kavli Institute of Cosmological Physics at the University of Chicago, the Center for Cosmology and Astro-Particle Physics at the Ohio State University, the Mitchell Institute for Fundamental Physics and Astronomy at Texas A&M University, Financiadora de Estudos e Projetos, Fundacao Carlos Chagas Filho de Amparo á Pesquisa do Estado do Rio de Janeiro, Conselho Nacional de Desenvolvimento Científico e Tecnológico and the Ministério da Ciência, Tecnologia e Inovacao, the Deutsche Forschungsgemeinschaft and the Collaborating Institutions in the Dark Energy Survey.

The DES data management system is supported by the U.S. NSF under grant AST-1138766. The DES participants from Spanish institutions are partially supported by MINECO under grants AYA2012-39559, ESP2013-48274, FPA2013-47986, and Centro de Excelencia Severo Ochoa SEV-2012-0234. Research leading to these results has received funding from the European Research Council under the European Union's Seventh Framework Programme (FP7/2007-2013) including ERC grant agreements 240672, 291329, and 306478. This research uses resources of the National Energy Research Scientific Computing Center, a DOE Office of Science User Facility supported by the Office of Science of the U.S. Department of Energy under Contract No. DE-AC02-05CH11231.

Software: astropy (Astropy Collaboration et al. 2013), Matplotlib (Hunter 2007), Numpy (Harris et al. 2020), Scipy (Virtanen et al. 2020), triangle v0.1.1. Zenodo. 10.5281/zenodo.11020

DATA AVAILABILITY STATEMENTS

The majority of the data have already been published and can be found in Poznanski et al. (2009) (KAIT-P09), D'Andrea et al. (2010) (SDSS-SN), de Jaeger et al. (2017a) (HSC), de Jaeger et al. (2019) (KAIT-d19), and de Jaeger et al. (2020a) (DES-SN). CSP-I and SNLS data will be shared on reasonable request to the corresponding author.

REFERENCES

Aihara H., et al., 2018, PASJ, 70, S4
Anand G. S., Rizzi L., Tully R. B., 2018, AJ, 156, 105
Anand G. S., Tully R. B., Rizzi L., Riess A. G., Yuan W., 2021, arXiv e-prints, p. arXiv:2108.00007
Astier P., Guy J., Regnault N., et al., 2006, A&A, 447, 31
Astropy Collaboration et al., 2013, A&A, 558, A33
Baxter E. J., Sherwin B. D., 2021, MNRAS, 501, 1823
Bellm E. C., et al., 2019, PASP, 131, 018002

Bennett C. L., Hill R. S., Hinshaw G., et al., 2003, ApJS, 148, 1
Bernstein J. P., Kessler R., Kuhlmann S., et al., 2012, ApJ, 753, 152
Blakeslee J. P., Jensen J. B., Ma C.-P., Milne P. A., Greene J. E., 2021, ApJ, 911, 65
Boruah S. S., Hudson M. J., Lavaux G., 2021, MNRAS, 507, 2697
Burns C. R., et al., 2018, ApJ, 869, 56
Carrick J., Turnbull S. J., Lavaux G., Hudson M. J., 2015, MNRAS, 450, 317
D'Andrea C. B., Sako M., Dilday B., et al., 2010, ApJ, 708, 661
Dessart L., Hillier D. J., 2005, A&A, 439, 671
Dhawan S., Jha S. W., Leibundgut B., 2018, A&A, 609, A72
Dhawan S., et al., 2022, arXiv e-prints, p. arXiv:2203.04241
de Jaeger T., González-Gaitán S., Anderson J. P., et al., 2015, ApJ, 815, 121
de Jaeger T., Galbany L., Filippenko A. V., et al., 2017a, MNRAS, 472, 4233
de Jaeger T., González-Gaitán S., Hamuy M., et al., 2017b, ApJ, 835, 166
de Jaeger T., et al., 2019, MNRAS, 490, 2799
de Jaeger T., et al., 2020a, MNRAS,
de Jaeger T., Stahl B. E., Zheng W., Filippenko A. V., Riess A. G., Galbany L., 2020b, MNRAS, 496, 3402
Di Valentino E., et al., 2021, arXiv e-prints, p. arXiv:2103.01183
Eastman R. G., Schmidt B. P., Kirshner R., 1996, ApJ, 466, 911
Filippenko A. V., Li W. D., Treffers R. R., Modjaz M., 2001, in Paczynski B., Chen W.-P., Lemme C., eds, Astronomical Society of the Pacific Conference Series Vol. 246, IAU Colloq. 183: Small Telescope Astronomy on Global Scales. p. 121
Fixsen D. J., Cheng E. S., Gales J. M., et al., 1996, ApJ, 473, 576
Foreman-Mackey D., Hogg D. W., Lang D., Goodman J., 2013, PASP, 125, 306
Freedman W. L., 2021, ApJ, 919, 16
Freedman W. L., Madore B. F., 2010, ARA&A, 48, 673
Freedman W. L., Madore B. F., Gibson B. K., et al., 2001, ApJ, 553, 47
Freedman W. L., et al., 2019, ApJ, 882, 34
Frieman J. A., Bassett B., Becker A., et al., 2008, AJ, 135, 338
Hamuy M., Pinto P. A., 2002, ApJ, 566, L63
Hamuy M., Folatelli G., Morrell N. I., et al., 2006, PASP, 118, 2
Harris C. R., et al., 2020, Nature, 585, 357
Huang C. D., et al., 2020, ApJ, 889, 5
Hubble E., 1929, Proceedings of the National Academy of Science, 15, 168
Humphreys E. M. L., Reid M. J., Moran J. M., Greenhill L. J., Argon A. L., 2013, ApJ, 775, 13
Hunter J. D., 2007, Computing in Science & Engineering, 9, 90
Jaffe A. H., Ade P. A., Balbi A., et al., 2001, Physical Review Letters, 86, 3475
Jang I. S., Lee M. G., 2017a, ApJ, 835, 28
Jang I. S., Lee M. G., 2017b, ApJ, 836, 74
Kanbur S. M., Ngeow C., Nikolaev S., Tanvir N. R., Hendry M. A., 2003, A&A, 411, 361
Kirshner R. P., Kwan J., 1974, ApJ, 193, 27
Kourkchi E., Tully R. B., Courtois H. M., Dupuy A., Guinet D., 2022, MNRAS,
Leavitt H. S., Pickering E. C., 1912, Harvard College Observatory Circular, 173, 1
Lee M. G., Freedman W. L., Madore B. F., 1993, ApJ, 417, 553
Lemaître G., 1927, Annales de la Société Scientifique de Bruxelles, 47, 49
Leonard D. C., Filippenko A. V., Li W., et al., 2002, AJ, 124, 2490
Leonard D. C., Kanbur S. M., Ngeow C. C., Tanvir N. R., 2003, ApJ, 594, 247
Li S., Casertano S., Riess A. G., 2022, arXiv e-prints, p. arXiv:2202.11110
Lindegren L., et al., 2021, A&A, 649, A2
Macaulay E., et al., 2019, MNRAS, 486, 2184
Madore B. F., Mager V., Freedman W. L., 2009, ApJ, 690, 389
McQuinn K. B. W., Skillman E. D., Dolphin A. E., Berg D., Kennicutt R., 2017, AJ, 154, 51
Miyazaki S., et al., 2012, Proc. SPIE, 8446, 84460Z
Olivares E. F., Hamuy M., Pignata G., et al., 2010, ApJ, 715, 833
Pesce D. W., et al., 2020, ApJ, 891, L1
Pietrzyński G., et al., 2019, Nature, 567, 200
Planck Collaboration et al., 2018, arXiv e-prints, p. arXiv:1807.06209
Polshaw J., et al., 2015, A&A, 580, L15
Poznanski D., Butler N., Filippenko A. V., et al., 2009, ApJ, 694, 1067
Reid M. J., Pesce D. W., Riess A. G., 2019, ApJ, 886, L27
Riess A. G., et al., 2009, ApJ, 699, 539
Riess A. G., Macri L., Casertano S., et al., 2011, ApJ, 730, 119
Riess A. G., Macri L. M., Hoffmann S. L., et al., 2016, ApJ, 826, 56
Riess A. G., Casertano S., Yuan W., et al., 2018a, ApJ, 855, 136
Riess A. G., et al., 2018b, ApJ, 861, 126
Riess A. G., Casertano S., Yuan W., Macri L. M., Scolnic D., 2019, ApJ, 876, 85
Riess A. G., et al., 2021a, arXiv e-prints, p. arXiv:2112.04510
Riess A. G., Casertano S., Yuan W., Bowers J. B., Macri L., Zinn J. C., Scolnic D., 2021b, ApJ, 908, L6
Rodríguez Ó., et al., 2019, MNRAS, 483, 5459
Sandage A., Tammann G. A., Saha A., Reindl B., Macchetto F. D., Panagia N., 2006, ApJ, 653, 843
Schmidt B. P., Kirshner R. P., Eastman R. G., et al., 1994, ApJ, 432, 42
Sedgwick T. M., Collins C. A., Baldry I. K., James P. A., 2021, MNRAS, 500, 3728
Spergel D. N., Bean R., Doré O., et al., 2007, ApJS, 170, 377
Van Dyk S. D., et al., 2019, arXiv e-prints,
Virtanen P., et al., 2020, Nature Methods, 17, 261
Vogl C., 2020, PhD thesis, Technical University of Munich, Germany
Vogl C., Sim S. A., Noebauer U. M., Kerzendorf W. E., Hillebrandt W., 2019, A&A, 621, A29
Vogl C., Kerzendorf W. E., Sim S. A., Noebauer U. M., Lietzau S., Hillebrandt W., 2020, A&A, 633, A88
Whitelock P. A., Feast M. W., Van Leeuwen F., 2008, MNRAS, 386, 313
Yuan W., Riess A. G., Macri L. M., Casertano S., Scolnic D. M., 2019, ApJ, 886, 61
Yuan W., et al., 2020, ApJ, 902, 26

This paper has been typeset from a TEX/LATEX file prepared by the author.